International Journal of Computer Applications (0975 - 8887)
Volume 187 - No.72, January 2026

A Deep Intuitionistic Fuzzy Clustering Framework for Multi-Stage Alzheimer's Disease

Sandhya Mohankumar
Department of Applied Mathematics
Bharathiar University
Coimbatore 641046, India

Dhanalakshmi Palanisami
Department of Applied Mathematics
Bharathiar University
Coimbatore 641046, India

Vethavigasini Deivasigamani
Government Medical College and Hospital, The Nilgiris
Udhagamandalam, India

ABSTRACT

This study proposes a structured, multi-phase framework to enhance medical image classification accuracy through early detection and precise classification of Azheimer's disease using MRI scans. Initially, image preprocessing using gaussian filtering and normalization is applied to suppress noise and standardize intensity levels. The proposed Deep Intuitionistic Fuzzy Clustering (DIFC) method effectively models uncertainty and vagueness inherent in medical imaging by incorporating membership, non-membership, and hesitation degrees, thereby achieving superior segmentation performance compared to traditional fuzzy clustering approaches. The Sea Lion Optimization Algorithm (SLOA) is employed to fine-tune clustering parameters, ensuring faster convergence and improved segmentation stability. Subsequently, textual, convolutional, and statistical features extracted from the segmented regions are optimized by Deep Maxout Network (DMN) using SLOA for multi-stage AD classification. Experimental results demonstrate that the proposed DIFC-SLOA-DMN framework achieves high accuracy, sensitivity, and specificity, validating its effectiveness as a robust and reliable computer-aided diagnostic system for early Alzheimer's disease detection and progression analysis.

Keywords

Classification, Deep intuitionistic fuzzy clustering, Sea lion optimization algorithm, Deep maxout network, Azhemeir's disease

1. INTRODUCTION

AD is one of the most widespread brain abnormalities in the elderly, particularly those over 60 years old and it is currently the fourth largest cause of death in developed countries. The primary symptom of this illness is a decline in thinking and memory, and severe AD will result in memory loss. Prescribed medication and memory-retention exercises can be administered if the condition is identified in its early stages, or we can assist the elderly in performing their daily tasks without difficulty [20]. AD progresses through various stages, beigning with the mild cognitive impairment (MCI) stage, which serves as the transitional stage between normal brain functions and AD [24]. In this context, early mild cognitive impairment (EMCI) emerges in the initial stages, while late mild cognitive impairment (LMCI) also refered as progressive mild cognitive impairment, is characterized by symptoms that progressively worsen. Subtle morphological changes in the brain leisons of patients in the MCI stage provides biomarkers for diagnosis and monitoring.
However identifying specific variations in symptoms across different subsets remains a significant challenge for researchers. To address these complexities, various medical imaging techniques, such as positron emission tomography, magnetic resonance imaging (MRI), and computed tomography, provide standardized testing protocols and imaging data for experimental analyses [10]. Among these, MRI is widely used due to its high resolution, good contrast, and ability to capture structural changes in the brain [7]. Structural MRI, in particular, plays a key role in detecting hallmark features such as atrophy in the medial temporal lobe, including the hippocampus and entorhinal cortex, which are critical for diagnosing AD and differentiating it from other forms of dementia [8].Techniques like ROI analysis and gray matter voxel morphometry are commonly applied to structural MRI data for AD diagnosis. Recent advancements in deep learning techniques have transformed the analysis of MRI data, significantly improving the accuracy and efficiency of AD diagnosis [6]. These models, known for their ability to automatically extract intricate features from complex datasets, have significantly enhanced the accuracy and efficiency of AD detection. Leveraging structural insights from MRI scans, deep learning models can identify subtle anatomical changes critical for early diagnosis and progression monitoring [3]. Techniques such as convolutional neural networks, recurrent neural networks, and autoencoders have shown remarkable potential in analyzing high-dimensional MRI data and classifying different stages of AD [5, 21]. To develop these advancements, optimization algorithms have been integrated with deep learning techniques to enhance model performance. Among these, the Sea Lion Optimization Algorithm (SLOA) has emerged as a promising method for hyperparameter tuning and improving training efficiency. By mimicking the social hunting behavior of sea lions, SLOA effectively balances ex-

ploration and exploitation, leading to better convergence, reduced training time, and improved classification accuracy [13].

Numerous studies have explored various innovative approaches for AD detection, focusing on leveraging advanced computational techniques and multimodal data analysis to improve diagnostic accuracy and efficiency. These efforts encompass a wide range of methodologies, including the application of machine learning, deep learning, optimization algorithms, and hybrid frameworks to process and analyze structural and functional imaging data. For the classification, Shankar et al. [17] proposed a hybrid method combining Group Grey Wolf Optimization with a convolutional classifier for feature selection, achieving notable improvements in classification performance. Adarsh et al. [15] integrated anatomical, diffusion, and resting-state functional MRI data to enhance individualized AD diagnosis, demonstrating the potential of multimodal imaging for better classification accuracy. Liu et al. [14] employed sparse logistic regression with spatial regularization for AD classification using structural MRI, providing a robust framework for feature selection. Zhang et al. [23] utilized a kernel support vector machine and decision tree for AD classification, leveraging structural imaging features to achieve significant accuracy improvements. ramya et al. [4] enhanced AD classification by combining multiple anatomical MRI measures, emphasizing the advantages of utilizing diverse structural imaging metrics. Aghajanian et al. [11] applied Locally Linear Embedding to MRI data for dimensionality reduction and feature extraction, showcasing the benefits of manifold learning techniques in AD diagnosis. Huang et al. [9] utilized voxel-based morphometry to distinguish early-stage AD from controls, laying the foundation for structural MRI analysis in AD research. Zhang et al. [22] addressed multiclass AD diagnosis using multimodal neuroimaging embedding feature selection and fusion, achieving state-of-the-art performance. Afzal et al. [2] presented a data augmentation framework to address class imbalance in AD stage detection, significantly improving classification accuracy and showcasing the role of augmentation in enhancing deep learning models for imbalanced datasets.

Building on these advancements, this study proposes a novel hybrid framework for the automated detection and classification of AD, focusing on the segmentation of critical brain regions and their classification using a DMN. This combination ensures precise delineation of the hippocampus, cerebral cortex, and ventricles, providing robust input for the classification phase. The brain regions are critical for memory and cognitive function, and their degeneration provides important biomarkers for disease progression. Accurate segmentation of these regions from MRI scans is a prerequisite for effective feature extraction and subsequent classification. Traditional segmentation techniques often struggle with noise, intensity inhomogeneity, and complex anatomical structures, necessitating more sophisticated approaches. One of the existing framework integrates the fuzzy clustering technique with advanced deep learning models has emerged as a promising approach in AD diagnosis. Techniques such as Fuzzy C-Means, Kernel-Based Fuzzy C-Means, Entropy-Weighted Fuzzy C-Means, and Spatial-Based Fuzzy C-Means are combined with deep learning models like Convolutional Neural Networks, Recurrent Neural Networks, and Deep Neural Networks to enhance the analysis of brain imaging data [26].

In this framework, the DIFC + SLOA-based DMN model is developed to overcome the limitations of existing methods. The Gaussian filter effectively removes image artifacts, enhancing accuracy, DIFC approach provides a robust framework for analyzing large-scale datasets. Accurate AD classification is achieved through effective feature extraction, and overfitting is mitigated using data augmentation techniques. Additionally, the DMN ensures fast convergence and optimal generalization of results.

1.1 Motivation

The accurate detection and classifying AD is still hard in medical imaging due to the complex and subtle changes in brain structure. Existing methods for segmenting and classifying things often not being able to generalise well, being inaccurate, or not being strong enough when used on different types of data. Moreover, many traditional approaches fail to leverage advanced optimization techniques to improve the precision of brain region segmentation and the reliability of classification models. The goal of this study is to fill in these gaps by creating a strong, automated system that can look at structural MRI images and make an early and accurate diagnosis of AD. This will help with making better treatments and giving better patient care.

Motivated by these problems, this study seeks to achieve the following objectives:

(1) To design an optimal segmentation model capable of effectively handling sparse datasets.
(2) Integrating proposed DMN with optimized SLOA classifies the images into five stages such as AD, MCI, EMCI, LMCI and CN.
(3) To demonstrate the efficacy of the SLOA in enhancing both segmentation and classification tasks, with a particular focus on optimizing hyperparameters, improving convergence rates, and ensuring the precise identification of subtle structural and morphological changes in the brain.
(4) Through comparison with existing methods such as DFC+CNN and DFC+SLDHOA, shows significant improvements in accuracy, sensitivity, and specificity, which highlights the superiority of the proposed framework.

2. METHODOLOGY

The proposed methodology comprises the steps including image processing, region of interest, segmentation by DIFC with SLOA and also classifying the images. The process begins with acquiring a noisy MRI image, which undergoes pre-processing techniques such as filtering and enhancement where filtering eliminates noise, while enhancement improves the image's contrast. Further, it is subjected to image segmentation to isolate the ROI. Features are subsequently extracted from these segmented regions. After the dimensionality reduction of the extracted features, the image is classified into their respective categories. The steps involved in this methodology, from dimensionality reduction to classification, are illustrated in the workflow shown in Fig 1.

2.1 Dataset Description

Alzheimer's Disease Neuroimaging Initiative (ADNI) dataset which consists of neuroimaging data, including MRI scans, which are used for the analysis and classification of AD. The dataset includes different stages of cognitive impairment associated with AD. Consider the ADNI dataset as M and it is mathematically represented as $M = N_1, N_2, \ldots, N_i, \ldots, N_h$ where M denotes the dataset, h denotes the number of images and N_i denotes the i^{th} image of the input.

2.2 Preprocessing dataset

Here, the preprocessing stage involves noise reduction in the dataset by using the Gaussian filter. It operates based on the Gaus-

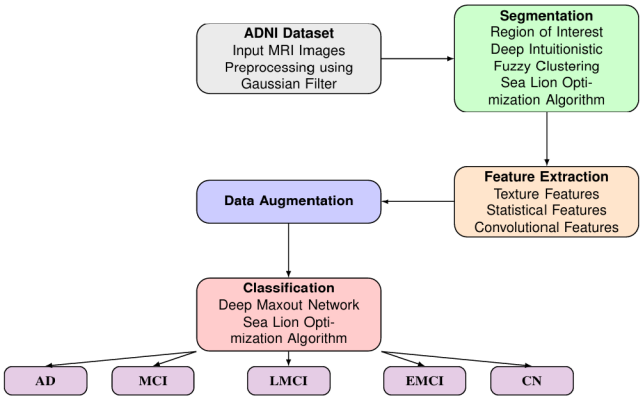

Fig. 1. Structure of Proposed AD segmentation and classification

sian function, which calculates a weighted average of surrounding pixels, assigning greater weight to central pixels. This function is represented as

$$G(p,q) = \frac{1}{\sqrt{2\pi\sigma^2}} e^{(-\frac{p^2+q^2}{2\sigma^2})} \tag{1}$$

where p and q are the points in the coordinates of the filter kernel, σ is the standard deviation.

2.3 Region of interest in segmentation

ROI in segmentation increases the focus on relevant brain regions, thus improving the detection and classification of AD. By isolating specific areas for analysis, the process reduces computational complexity and enhances the accuracy of feature extraction, ultimately leading to better classification performance in the subsequent deep learning models [18]. The ROI in segmentation starts with the preprocessed brain MRI image, which has undergone Gaussian filtering to reduce noise and improve image quality. It is enhanced using a DIFC process and optimized by the SLOA. DIFC helps in handling uncertainty and soft boundaries, where each pixel has membership, non-membership, and hesitation degrees to different clusters. This flexibility allows a better definition of borders between brain regions, improving segmentation accuracy. SLOA fine-tunes the hyperparameters of the clustering process, such as the number of clusters and the fuzziness coefficient, to improve the segmentation quality. This optimization ensures that the clusters correspond to meaningful anatomical structures in the brain, enhancing the accuracy of the segmentation. After clustering the regions affected by AD are identified as ROI.

2.4 Proposed DIFC-DMN Algorithm

Algorithm 1: DIFC-DMN for Alzheimer's Disease Classification
Input: Raw MRI images M
Output: Classified Alzheimer's disease stages

(1) Load MRI dataset M.
(2) Initialize index $i = 0$.
(3) While $i < |M|$, perform the following:
  (a) Apply Gaussian filtering to remove noise.
  (b) Normalize pixel intensities to the range $[0, 1]$.
  (c) Generate intuitionistic fuzzy representation.
  (d) Increment $i = i + 1$.
(4) Obtain preprocessed image set M_p.
(5) Initialize sea lion population as candidate DIFC cluster centers.
(6) Set iteration counter $t = 0$.
(7) While $t < T_{\max}$, perform:
  (a) Update positions using spiral encircling and random wandering.
  (b) Compute fitness based on intra-cluster variance and entropy.
  (c) Update DIFC cluster centers adaptively.
  (d) Increment $t = t + 1$.
(8) Segment M_p into regions of interest to obtain M_s.
(9) Extract CNN features from M_s using convolution and pooling layers.
(10) Initialize sea lion population for DMN hyperparameter optimization.
(11) While convergence is not reached:
  (a) Update hyperparameters.
  (b) Evaluate classification accuracy.
(12) Train the DMN with optimal hyperparameters.
(13) Evaluate performance using accuracy, sensitivity, and specificity.
(14) Return final classification results.

2.5 Deep Intuitionistic Fuzzy clustering

In this research, DIFC provides an approach for segmenting and classifying AD in brain imaging by integrating IFC within deep neural networks, allowing it to extract complex, high-level features from data automatically. After the preprocessing stage, the outputs of preproccessed images are used as input for the process of DIFC. The DIFC is formulated by integrating the clustering process with the SLOA algorithm, enabling the SLOA to optimize the clustering process effectively. The process involves dividing the samples M into m/m_c batches, with each batch containing a training image $N_i, i = 1, 2, ..., m/m_c$. During training, the autoencoder utilizes weights ω and biases D, while λ is chosen as the intuitionistic fuzzy clustering center. The hidden features are denoted as Q_v, while memberships are represented as I_v. Pseudo-labels are also calculated as I_v, which are used to initialize the affinities across all batches, $L_v \in R^{m_c \times m_c}$. This process ensures a more robust representation of clustering by incorporating both fuzzy and intuitionistic principles, improving segmentation precision and adaptability. The loss function for DIFC is expressed as,

$$O(K_\theta) = \frac{1}{m} \sum_{i=1}^{m} \|x_{E,S}(M_i) - M_i\|^2 + \eta \cdot \Upsilon(E) \tag{2}$$

Here, $\|\cdot\|$ denotes the Euclidean norm, $\Upsilon(E)$ represents the regularization term, and $x_{E,S}(M_i)$ denotes the reconstruction term. Let $g_i \in R^q$ represent the hidden feature vector, and let $Q_v = \{g_1, g_2, \ldots, g_m\}$ denote the set of hidden features. In the intuitionistic fuzzy clustering layer, the input g_i, the membership degree R_{ij}, and the non-membership degree S_{ij} are defined as follows:

$$R_{ij} = \frac{\left(\|g_i - \lambda_j\|^2 - \frac{\gamma}{\sum_{\tau=1}^{q} \|\lambda_\tau - \bar{\lambda}\|^2} \|\lambda_j - \bar{\lambda}\|^2 \right)^{-\frac{1}{a-1}}}{\sum_{\tau=1}^{q} \left(\|g_i - \lambda_\tau\|^2 - \frac{\gamma}{\sum_{\tau=1}^{q} \|\lambda_\tau - \bar{\lambda}\|^2} \|\lambda_\tau - \bar{\lambda}\|^2 \right)^{-\frac{1}{a-1}}} \tag{3}$$

$$S_{ij} = 1 - R_{ij} - T_{ij}, \quad T_{ij} \leq 1 - (R_{ij} + S_{ij}) \tag{4}$$

where γ is the hyperparameter controlling cluster distance and space, a is the fuzzification parameter, and T_{ij} is the hesitation degree, ensuring that $R_{ij} + S_{ij} + T_{ij} = 1$.
Pseudo-labels I_v and targets M are calculated as:

$$M_{ij} = \frac{R_{ij}^2}{\sum_i R_{ij}} \Bigg/ \sum_{\tau=1}^{q} \left(\frac{R_{i\tau}^2}{\sum_i R_{i\tau}} \right), \quad \sum_{j=1}^{q} M_{ij} = 1 \quad \forall i \tag{5}$$

The loss function for KL-divergence is modified to incorporate intuitionistic fuzzy principles:

$$\min KL(M\|I) = \min \sum_{i=1}^{m} \sum_{j=1}^{q} \left(M_{ij} \log \frac{M_{ij}}{R_{ij}} + S_{ij} \log \frac{S_{ij}}{1 - R_{ij}} \right) \tag{6}$$

Graph regularization is represented as:

$$\min H_g = \min \sum_{i,l=1}^{m} \|g_i - g_l\|^2 e_{il} \tag{7}$$

where e_{il} denotes the affinity between M_i and M_l. High affinity reduces the distance between h_i and g_l, minimizing the regularization.
Finally, the overall loss function B for DIFC is expressed as: B = $\sum_{i=1}^{m} \|x_{E,S}(h_i) - h_i\|^2$
$+ \beta_1 \sum_{i=1}^{m} \sum_{j=1}^{q} \left(M_{ij} \log \frac{M_{ij}}{R_{ij}} + S_{ij} \log \frac{S_{ij}}{1-R_{ij}} \right)$
$+ \beta_2 \sum_{i=1}^{m} \sum_{l=1}^{m} \|g_i - g_l\|^2 \, e_{il}$.
where:

$$e_{il} = \{ \ \exp\left(-\|g_i - g_l\|^2/\kappa\right)\chi, \ell_i = \ell_l, 0, \ell_i \neq \ell_l. \tag{8}$$

The hyperparameters $\beta_1, \beta_2, \gamma, \chi$, fuzzifier m and ℓ_i, ℓ_1 expresses the labels of DIFC are optimized using the SLOA.

2.6 Sea Lion Optimization Algorithm

SLOA is a global optimization algorithm inspired by the hunting behaviors of sea lions, including their encircling and prey-capturing techniques, as well as their use of tails and whiskers. SLOA has demonstrated competitive performance compared to establish particle swarm optimization algorithms across various benchmark functions. SLOA is used to optimize the hyperparameters of the DIFC framework, ensuring improved clustering accuracy, better assignment, and faster convergence. The following steps outline the process of SLOA. [13]

2.6.1 Initialization Phase. At first, SLOA begins by generating an initial population of solutions in a D-dimensional search space. This population represents the possible positions of sea lions, initialized randomly within the defined boundaries:

$$X_{i,j}^{init} = X_{i,j}^{min} + rand_{i,j} \cdot (X_{i,j}^{max} - X_{i,j}^{min}) \tag{9}$$

where $i = 1, 2, \ldots, N$, $j = 1, 2, \ldots, D$, $X_{i,j}^{init}$ is the initial position vector of the i-th solution, $X_{i,j}^{min}$ and $X_{i,j}^{max}$ denote the minimum and maximum bounds for the j^{th} dimension of the i^{th} solution, $rand_{i,j}$ is a uniform random value in the interval $[0, 1]$.

2.6.2 Detecting and Tracking Phase. The fitness of each sea lion's position is evaluated using the objective function. The best-performing solution, $X_{best}^{(t)}$, is identified. Other sea lions adjust their positions based on $X_{best}^{(t)}$ using the encircling mechanism:

$$X^{(t+1)} = X_{best}^{(t)} - C \cdot \left| 2r \cdot X_{best}^{(t)} - X^{(t)} \right| \tag{10}$$

where $X_{best}^{(t)}$ is the position vector of the best solution at iteration t, $X^{(t)}$ is the position vector of a sea lion in iteration t, t is the current iteration, t_{max} is the maximum number of generations, r is a random value in the range $[0, 1]$, C encircling coefficient multiplied by 2 to increase the search range, $C = 2\left(1 - \frac{t}{t_{max}}\right)$ and linearly decreases from 2 to 0 across iterations.

2.6.3 Vocalization Phase. When a sea lion recognizes prey (e.g., fish), it calls other group members to form a net for capturing. This is modeled using the leader's signal:
$\text{SP}_{leader} = \left| \frac{V_1(1+V_2)}{V_2} \right|$
$V_1 = \sin(\theta)$
$V_2 = \sin(\phi)$
where SP_{leader} represents the leader's decisions, $\theta = 2\pi r$ is the angle of voice reflection, $\phi = 2\pi(1 - r)$ is the angle of voice refraction, r is a random number in the range $[0, 1]$.

2.6.4 Attacking Phase (Exploitation Phase). The leader sea lion leads the hunting process in two key phases:

(1) Dwindling Encircling Technique: The encircling mechanism (controlled by C) allows the search space to shrink, focusing the search agents around the best solution.
(2) Circling Updating Position: The position of a sea lion is updated using:

$$X^{(t+1)} = X_{best}^{(t)} + \cos(2\pi m) \cdot \left| X_{best}^{(t)} - X^{(t)} \right| \tag{11}$$

where m is a random number in the range $[-1, 1]$.

2.6.5 Searching for Prey (Exploration Phase). When $C > 1$, sea lions prioritize exploration by moving towards randomly selected solutions to avoid premature convergence. This is described by:

$$X^{(t+1)} = X_{rand}^{(t)} - C \cdot \left| r \cdot X_{rand}^{(u)} - X^{(t)} \right| \tag{12}$$

where $X_{rand}^{(u)}$ is the position vector of a randomly selected sea lion, r is a random value in $[0, 1]$ and this phase

2.6.6 Update best solution. The best solution is identified, and all sea lions adjust their positions toward it. The above algorithm iterates until the maximum number of iterations u_{max} is reached.

2.7 Feature extraction

The features are extracted from the segmented images for the process of classification. This extraction includes texture features, statistical features and the convolutional features which are dicussed below.

Table 1. Statistical features with their mathematical formulations

Statistical Feature	Mathematical Expression
Mean (V_3)	$V_3 = \frac{1}{N}\sum_{x,y} I(x,y)$
Variance (V_4)	$V_4^2 = \frac{1}{N}\sum_{x,y}(I(x,y) - V_3)^2$
Standard Deviation (V_5)	$V_5 = \sqrt{\frac{1}{N}\sum_{x,y}(I(x,y) - V_3)^2}$
Energy (V_6)	$V_6 = \sum_{x,y} I(x,y)^2$
Entropy (V_7)	$V_7 = -\sum_i p_i \log_2(p_i)$
Contrast (V_8)	$V_8 = \sum_{x,y}(x-y)^2\, p(x,y)$
Kurtosis (V_9)	$V_9 = \frac{\frac{1}{N}\sum_{x,y}(I(x,y)-V_3)^4}{V_5^4}$
Skewness (V_{10})	$V_{10} = \frac{\frac{1}{N}\sum_{x,y}(I(x,y)-V_3)^3}{V_5^3}$

2.7.1 Texture features. The texture features are extracted from segmented regions from the methods of Local Gabor Binary Pattern (LGBP) and Symmetric Local Information Pattern (SLIP). The methods are as follows, (i) LGBP: It is a texture descriptor that captures local texture information by combining Gabor filters with binary pattern encoding. The Gabor filters capture different frequency and orientation responses, allowing for the extraction of multi-scale texture features and capable of capturing significant texture information from brain images. (ii) SLIF: It is another method that analyzes the local intensity values of pixels within a local neighborhood and captures variations in texture. This method is particularly effective for identifying patterns in brain images associated with different stages of AD.

2.7.2 Statistical features. The statistical features play a vital role in analyzing and are used to enhance deep learning techniques for classification. The features are, (iii)Mean: Mean value represents the average pixel intensity within a region. It helps the overall brightness and texture of the image. (ii)Variance: It measures the spread of pixel values around the mean. High variance indicates significant texture, while low variance suggests smoother areas. (iv)Standard Deviation: The square root of variance, quantifies the variation in pixel intensity. A higher standard deviation often reflects greater contrast. (v)Energy: Calculated as the sum of squared pixel values, energy reflects the amount of textures and high energy values correlated. (vi)Entropy: A measure of the unpredictability in the intensity distribution, higher entropy values indicate more complex textures. This can be particularly useful in distinguishing between different stages of cognitive impairment. (vii)Contrast: Assesses the difference in intensity between neighboring pixels and higher contrast indicates sharper distinct features. (viii)Kurtosis: Measures the "tailedness" of the intensity distribution. High kurtosis indicates more extreme values and significant textural patterns. (ix)Skewness: Indicates the asymmetry of the distribution of pixel intensities. Positive skewness means a longer tail on the right side of the distribution gives the brighter pixels, while negative skewness indicates the opposite distribution gives the darker pixels. The mathematical formulas for the respective statistical features are described in Table 1

2.7.3 CNN features. CNN feature is one of the neural network models, which plays a vital role in extracting the features and it precisely identifies and localizes the ROI by recognizing the patterns of the affected brain regions. It contains 4 input layers, 4 max pooling layers, 4 convolutional layers, and 3 dense layers with the activation functions of softmax and relu. The above-mentioned

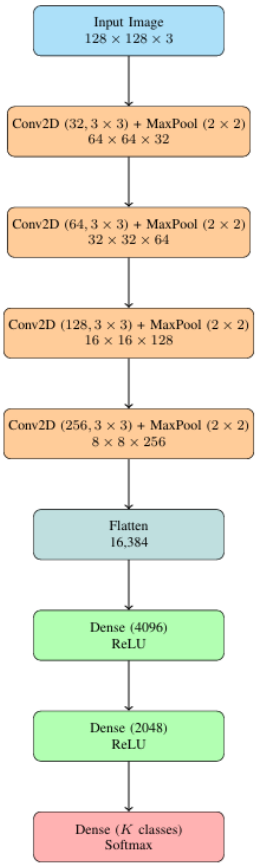

Fig. 2. Overall architecture of the proposed system

structure in flowchart2 extracts the feature and is fed into the DIFC process with SLOA to refine the segmentation results. The convolutional layer segments, denoted as J, serve as the input, while the CNN features are the output, represented by C with a dimension of $[1 \times 2048]$. The output function of the convolutional operation is mathematically expressed as:

$$P(k) = (p * C(k)) \tag{13}$$

where p represents the input to the CNN, $P(k)$ is the resulting feature map, and $C(k)$ denotes the kernel or probability density function applied during convolution.
The features are characterized into vectors V such as V=$\{V_1, V_2, V_3, V_4, V_5, V_6, V_7, V_8, V_9, V_{10}\}$ where V_1 refers LGBP, V_2 refers SLIF, V_3 refers mean, V_4 refers variance, V_5 refers standard deviation, V_6 refers energy, V_7 refers entropy, V_8 refers contrast, V_9 refers kurtosis, V_{10} refers skewness.

2.8 Data augmentation

The vector features V is fed into a data augmentation module that employs several key techniques: feature standardization, zero-phase component analysis (ZCA), and random rotations, flips, and shifts[19]. In feature standardization, features are normalized to have zero mean and unit variance, ensuring a consistent data distribution across the training set. ZCA is applied to decorrelate the input features and reduce redundancy while preserving the original

spatial structure, thereby enhancing the independence of features and making the model more robust to noise and variations[12]. Additionally, random rotations, shifts, and flips are performed to simulate different viewpoints and orientations, which helps reduce overfitting by exposing the model to a broader range of data variations.

2.9 AD classification

The classification process begins with input derived from the segmented regions of the images. These segmented images are subsequently used in a data augmentation process to enhance the robustness of the dataset. The augmented images are then fed into the classification framework, which employs a deep maxout network optimized using the SLOA and the evaluation metrics which are used to adjust the AD classification. After training, the performance of the classifier is evaluated using a confusion matrix from which the following metrics are evaluated:

(1) Accuracy: Measures the overall correctness of the model by comparing the number of correct predictions to the total number of predictions.

$$Accuracy = \frac{TP + TN}{TP + TN + FP + FN} \tag{14}$$

(2) Sensitivity (Recall): Indicates the model's ability to correctly identify positive cases. It is the ratio of true positives to the sum of true positives and false negatives.

$$Sensitivity = \frac{TP}{TP + FN} \tag{15}$$

(3) Specificity: Reflects the model's ability to correctly identify negative cases. It is calculated as the ratio of true negatives to the sum of true negatives and false positives.

$$Specificity = \frac{TN}{TN + FP} \tag{16}$$

3. EXPERIMENTAL RESULTS

The proposed DIFC+SLOA with DMN is evaluated for accuracy, specificity and sensitivity for varying training datas. By utilizing the Alzheimer's Disease-5-Class-Dataset-ADNI [1], which consists of MRI images arranged into two directories and classified into the five stages of AD, namely AD, MCI, LMCI, EMCI, and CN, are used in the analysis.

3.1 Evaluation of Segmentation

The evaluation of segmentation results using the proposed DIFC optimized by the SLOA is discussed below. The dataset was preprocessed using a Gaussian filter to reduce noise and improve image quality. Subsequently, the DIFC algorithm with SLOA was employed to segment critical regions and Fig 3.1 illustrates the segmentation includes the original image, the original mask, the whole brain abnormality mask, the hippocampus mask and the enlarged ventricles mask. Additionally, it presents a blank mask, which signifies the absence of regions to cluster in the cortical atrophy. The proposed DIFC+SLOA model achieved an outstanding accuracy of 0.993, and surpassing the previous DFC+SLDHOA approach, which yielded an accuracy of 0.826. Additionally, the proposed model exhibited a minimal loss value of 0.0623, emphasizing improved segmentation performance compared to traditional DFC methods as depicted in Fig 4, which shows the accuracy and loss of both training and validation datasets.

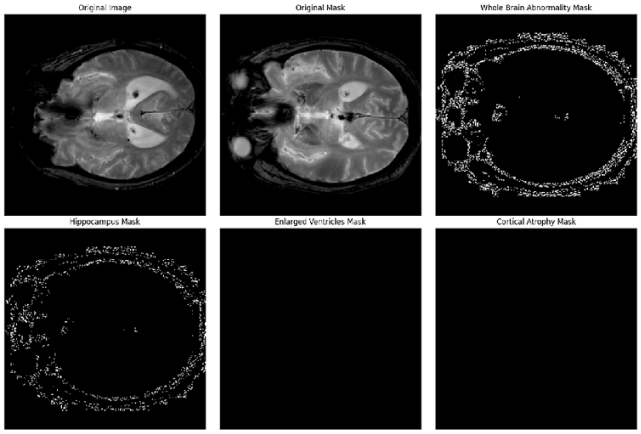

Fig. 3. Mask images for segmentation

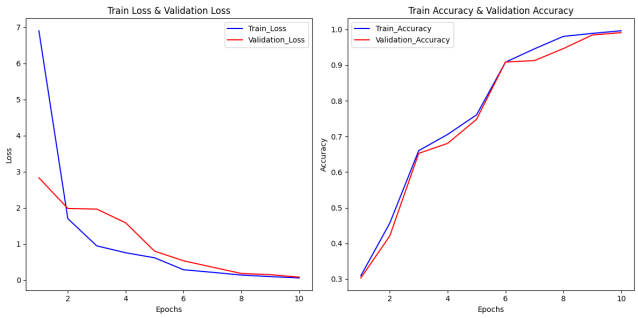

Fig. 4. Loss and Accuracy of Training and Validation dataset

3.2 Evaluation of Classification

After segmentation, features are extracted, and data augmentation is applied for the classification of AD. These features are used as input to the DMN optimized with the SLOA. The proposed model classifies AD by evaluating accuracy, sensitivity, and specificity metrics derived from the confusion matrix.The below Table 2 provides the results various AD detection methods.

Table 2. Comparison of different methods for AD detection

Method	Accuracy (%)	Sensitivity (%)	Specificity (%)
DFC + RF	75.9	75.9	86.1
DFC + CNN	76.4	80.8	88.0
TL + CNN	78.4	83.6	87.3
DFC + SLDOA + DMN	79.1	83.9	**88.8**
Proposed: DIFC + DMN	**86.9**	**96.72**	86.9

In comparison to existing methods Fig.3.2, DFC+CNN [3] achieved an overall accuracy of 76.8%, sensitivity of 80.8%, and specificity of 88.0%. Similarly, the DFC+SLDHOA method [18] reported an overall accuracy of 79.1%, sensitivity of 83.9%, and specificity of 88.8%.

The proposed model demonstrates a significant improvement with an overall accuracy of 86.90%, reflecting the model's overall correctness. The **sensitivity of 96.72%** highlights the model's exceptional ability to **identify positive cases**, while the specificity of 86.90% underscores its capability to correctly classify non-positive cases. Fig 3.2 illustrates the predicted results of AD using TP, TN,

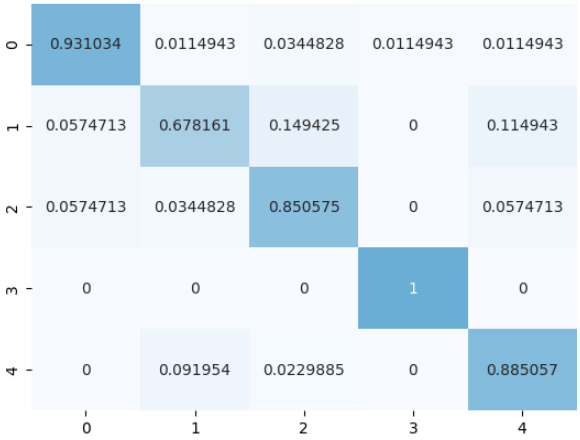

Fig. 5. Performance of model to classify AD

FP, and FP metrics. Fig 3.2 displays the dataset results, categorizing correctly predicted cases into AD, LMCI, EMCI, MCI, and CN classes.

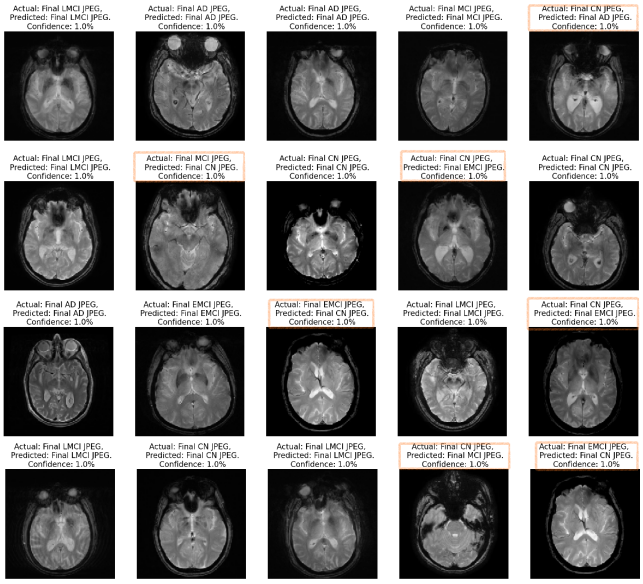

Fig. 6. Performance of model to classify AD

4. COMPARATIVE ANALYSIS OF DIFFERENT OPTIMIZATION ALGORITHM

In this study, Alzheimer's disease detection was initially performed using the SLOA for both segmentation and classification tasks. To further validate and benchmark the effectiveness of the proposed framework, we extended the process by employing Grey Wolf Optimization (GWO) and Particle Swarm Optimization (PSO).

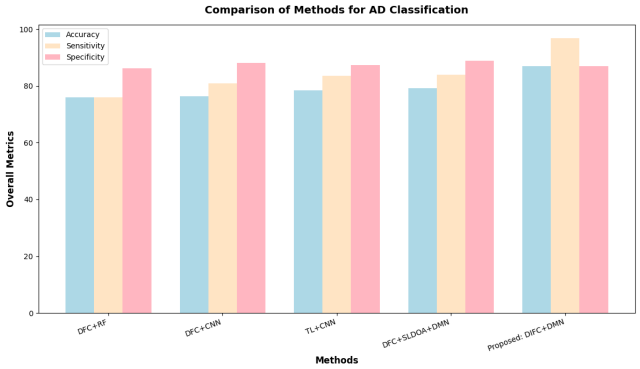

Fig. 7. Overall Metrics with different algorithms

4.1 Grey Wolf Optimization (GWO)

The **Grey Wolf Optimizer (GWO)** is inspired by the social hierarchy and hunting behavior of grey wolves in nature. In this algorithm, the three best solutions are considered as leader wolves- $\alpha_1, \beta_1, \delta_1$-which guide the remaining wolves, called ω_1 wolves, toward promising regions in the search space to find the global optimum. The hunting process in GWO consists of three main steps: *encircling, hunting, and attacking the prey*.

(1) Encircling: Wolves surround the prey, which can be mathematically modeled as:

$$F = |D \cdot X_{p1} - X_1|, \quad X_1(t+1) = X_{p1} - A \cdot F \tag{17}$$

where X_p is the prey position, X is the wolf position vector at iteration t, and A and C are coefficient vectors calculated as:

$$A = 2a \cdot r_1 - a, \quad F = 2r_2 \tag{18}$$

Here, $r_1, r_2 \in [0, 1]$ are random vectors, and a decreases linearly from 2 to 0 over iterations to balance exploration and exploitation.

(2) Hunting: It is assumed that α, β, δ have better knowledge of the prey's location. Therefore, the other wolves follow these leaders. The hunting behavior is described by: $\mathrm{F}_{\alpha_1} = |D_1 X_{\alpha_1} - X_1|$,
$F_{\beta_1} = |D_2 X_{\beta_1} - X_1|$,
$F_{\delta_1} = |D_3 X_{\delta_1} - X_1|$,
$X_1 = X_{\alpha_1} - A_1 F_{\alpha_1}$,
$X_2 = X_{\beta_1} - A_2 F_{\beta_1}$,
$X_3 = X_{\delta_1} - A_3 F_{\delta_1}$,
$X(t+1) = \frac{X_1 + X_2 + X_3}{3}$.
where $X_\alpha, X_\beta, X_\delta$ are the positions of the top three wolves, and A_1, A_2, A_3 and D_1, D_2, D_3 are calculated similarly to A and D.

(3) Attacking: The hunting concludes when the prey stops moving. Wolves then move toward the prey's position for exploitation. The coefficient a continues to decrease linearly, controlling the transition from exploration to exploitation. Typically, the first half of iterations focuses on exploration, while the latter half emphasizes exploitation, allowing wolves to refine their positions between their current location and the prey.

4.1.1 *Applications in AD Detection Pipeline*

(1) Segmentation:In segmentation optimizes DIFC cluster centers and fuzzifier values for accurate, noise-robust brain MRI segmentation.
(2) Classification: In classification fine-tune DMN hyperparameters (e.g., number of layers, neurons, learning rate) to maximize AD stage classification accuracy.
(3) Uncertainty-aware optimization: Performs well in complex, high-uncertainty medical imaging environments.

4.2 Particle Swarm Optimization (PSO)

The **Particle Swarm Optimization (PSO)** algorithm is inspired by the social behavior of bird flocking and fish schooling. In PSO, each particle represents a candidate solution and moves through the search space by updating its velocity and position based on both its own experience and the experience of the swarm. Each particle keeps track of its *personal best* position ($pbest$) and the *global best* position ($gbest$) found by the swarm.

(1) Velocity Update: The velocity of particle i at iteration $t+1$ is updated as follows:

$$v_i^{t+1} = \omega v_i^t + c_1 r_1 (pbest_i - x_i^t) + c_2 r_2 (gbest - x_i^t) \quad (19)$$

where:
(a) v_i^t is the current velocity of particle i,
(b) x_i^t is the current position of particle i,
(c) ω is the inertia weight controlling exploration and exploitation,
(d) c_1, c_2 are acceleration coefficients for personal and global learning,
(e) $r_1, r_2 \sim U(0,1)$ are random numbers.

(2) Position Update: The position of particle i is then updated according to:

$$x_i^{t+1} = x_i^t + v_i^{t+1} \quad (20)$$

4.2.1 Properties of PSO

(1) Particles share information about their best positions to guide the swarm toward optimal solutions.
(2) The inertia weight ω balances global exploration and local exploitation.
(3) PSO converges rapidly but may risk premature convergence if diversity in the swarm is low.

4.2.2 Application in AD Detection Pipeline. In the Alzheimer's Disease (AD) detection framework:

(1) Segmentation (DIFC optimization): Each particle encodes a possible set of DIFC cluster centers and fuzzifier values. Particles move in the search space to minimize the DIFC objective function, resulting in optimal segmentation of brain MRI images.
(2) Classification (DMN optimization): PSO can also be used to optimize DMN hyperparameters for improved classification accuracy.

To ensure a comprehensive evaluation, the proposed model was further executed using the Grey Wolf Optimizer (GWO) and Particle Swarm Optimization (PSO) algorithms. The comparative outcomes are presented in Table 3, while a consolidated summary of the overall segmentation and classification performance is reported in Table 4.
As shown in Table 3, SLOA consistently achieves superior performance across multiple evaluation metrics. Specifically, SLOA provides the highest classification accuracy (86.9%) compared to GWO (80.8%) and PSO (82.6%), indicating greater reliability in detecting AD stages. Similarly, SLOA demonstrates exceptional sensitivity (96.72%), ensuring that AD-positive cases are identified with minimal false negatives. Although both GWO and PSO yield relatively high specificity (88.8%), SLOA achieves a better balance by combining strong specificity with significantly higher sensitivity.
In terms of computational efficiency, PSO converges fastest (1.2 s/epoch), but its performance is undermined by premature convergence, which reduces accuracy and robustness. GWO, while offering stronger global search ability, suffers from slower convergence (2.4 s/epoch). In contrast, SLOA achieves an effective trade-off with moderate computation time (1.8 s/epoch), while maintaining superior accuracy and sensitivity, making it the most reliable choice for medical imaging tasks.

Table 3. Comparison of SLOA, GWO, and PSO for AD segmentation and classification

Optimizer	Acc. (%)	Sens. (%)	Spec. (%)	Time (s/epoch)
SLOA	86.9	96.72	86.9	1.8
GWO	80.8	79.1	88.8	2.4
PSO	82.6	89.5	88.8	1.2

Table 4. Comparison of SLOA, GWO, and PSO for AD detection pipeline

Stage	SLOA Advantage	GWO	PSO
Segmentation	Optimal DIFC cluster centers; robust to noise	Good cluster selection; slower	Fast; may trap in local optima
Classification	Efficient DMN hyperparameter tuning	Effective but slower	Fast, less stable accuracy
Overall	Best trade-off of accuracy and robustness	Moderate performance	Fast but sensitive to noise

Experimental results presented in Table 3 further reinforce these findings. While PSO provides faster convergence, its tendency to become trapped in local optima reduces its reliability in noisy medical imaging datasets. GWO offers better global search capabilities and competitive accuracy but at the cost of increased computation time. By contrast, SLOA achieves the most favorable balance between segmentation accuracy, classification robustness, and computational efficiency, making it the most effective optimization strategy for Alzheimer's Disease detection.

4.3 Ablation Study

The ablation study was conducted to systematically evaluate the contribution of each component in the proposed DIFC+SLOA+DMN for AD classification using MRI images. The objective was to determine the impact of fuzzy preprocessing, segmentation with DIFC, and classification using the DMN. To this end, we compared the baseline method TL+CNN with our proposed approach (DIFC-DMN).
The results clearly demonstrate the effectiveness of fuzzy preprocessing and DIFC-based segmentation. The TL+CNN baseline achieves an accuracy of 78.4%, sensitivity of 83.6%, and specificity of 88.8%. In contrast, the proposed DIFC+DMN achieves a significantly higher accuracy of 86.9% and sensitivity of 96.72%, while maintaining comparable specificity (86.9%). From the Table5 the findings emphasize role of fuzzy preprocessing, contibution of DIFC segmentation and the impact in classification.

(1) Role of fuzzy preprocessing: Gaussian filtering, intensity normalization, and intuitionistic fuzzy representation enhance

Table 5. Ablation study performance of DIFC+DMN

Method	Accuracy (%)	Sensitivity (%)	Specificity (%)
Without DIFC	78.4	83.6	**88.8**
With DIFC	**86.9**	**96.72**	86.9

cluster separability, thereby improving segmentation reliability and downstream classification.

(2) Contribution of DIFC segmentation: Replacing DIFC with conventional clustering reduces segmentation fidelity, which negatively impacts classification metrics.

(3) Impact of classification model: Using CNN features without DMN compromises stage discrimination, highlighting the importance of the DMN's representation learning and SLOA-based hyperparameter optimization.

Thus, the integration of fuzzy preprocessing, DIFC for segmentation, and DMN for classification is crucial to achieving robust and precise AD detection. The ablation study validates that each component contributes to the overall performance improvement of the proposed DIFC+DMN.

5. DISCUSSION

Although our model demonstrates outstanding performance overall, as analyzed above, it still exhibits deficiencies when diagnosing certain intermediate stages of AD, particularly in distinguishing between EMCI and LMCI. Therefore, we consider the current model suitable only as an auxiliary diagnostic tool. Moreover, the current experiments are confined to MRI-based inputs from the ADNI dataset, so the model's capacity to generalize across different cohorts or modalities such as PET or CT scans remains to be verified. In light of these limitations, we propose that future work should focus on the following areas:

(1) **Enhancing Multi-Stage Discriminative Learning for AD Staging:** While the current framework effectively segments and classifies Alzheimer's stages using DIFC and SLOA, the challenge of classifying adjacent stages (e.g., EMCI vs. LMCI) still persists. Future models should adopt specialized stage-wise learning branches or attention mechanisms to emphasize subtle distinctions in progression stages.

(2) **Expanding Cross-Dataset, Multimodal, and Augmentation-Based Validation:** This study introduced a framework for the segmentation and classification of AD, demonstrating significant improvements in accuracy, sensitivity, and specificity. However, our current validation is confined to single-modality MRI data. In the future, we plan to incorporate additional imaging modalities—such as PET, CT, or DTI—to enhance classification accuracy through multimodal analysis. Furthermore, the use of advanced data augmentation techniques can be explored to artificially expand the training dataset and improve the model's robustness.

(3) **Scaling for Real-World Feasibility Using Larger and Diverse Datasets:** Efforts in future studies by training on such heterogeneous data, the model can gain robustness to variability seen in real-world clinical environments, improving its potential for deployment as a reliable diagnostic support tool.

(4) **Developing a Unified Fuzzy-Deep Diagnostic Platform:** Our current system applies deep learning and Intuitionistic fuzzy clustering sequentially. Future research should allow fuzzy logic to learn and propagate uncertainty-aware representations throughout the network, leading to more robust predictions under clinical ambiguities.

6. CONCLUSION

In this study, a novel framework for the segmentation and classification of AD using structural MRI images was presented. The proposed method combines DIFC with the SLOA for precise segmentation of critical brain regions such as the hippocampus, enlarged ventricles, and cortical areas. For classification, DMN optimized with SLOA was employed, effectively categorizing images into five stages of AD: CN, MCI, LMCI, EMCI, and AD. The integration of advanced segmentation techniques, feature extraction, data augmentation, and optimized deep learning models highlights the potential of the proposed framework in improving the diagnosis and staging of AD. This work not only provides a robust and reliable methodology for AD analysis but also demonstrates the importance of optimization algorithms in enhancing deep learning-based medical imaging systems. Furthermore, the segmentation accuracy achieved in this study surpasses baseline limitations, with the proposed model reaching a high accuracy of 0.972 for larger datasets, a significant improvement over the previously reported value of 0.826. Unlike prior work, which suffered from poor generalization due to limited datasets, the proposed framework leverages a larger dataset to enhance robustness and reliability. By integrating DIFC with SLOA, this method ensures precise region segmentation, overcoming challenges faced by earlier approaches and contributing to improved AD analysis and classification.

6.1 Future Direction

To enhance the robustness, generalization, and clinical applicability of the proposed framework, future research could focus on integrating multimodal neuroimaging datas using attention-based fusion and graph neural networks to capture complementary biomarkers for more accurate and reliable diagnosis. Advanced data augmentation techniques, including Generative Adversarial Networks (GANs), diffusion models, and various transformations, can generate realistic synthetic data, increasing dataset diversity and improving generalization. In parallel, transformer-based and hybrid CNN-RNN architectures can be leveraged to model complex spatial and temporal dependencies, further enhancing segmentation and classification performance. Together, these advancements aim to expand the framework's capability to detect a wider range of neurodegenerative diseases and support its practical integration into real-world healthcare systems.

7. REFERENCES

[1] Alzheimer's Disease 5-Class Dataset (ADNI), available at: *https://www.kaggle.com/madhucharan/alzheimersdisease 5classdatasetadni*, accessed July 2021.

[2] S. Afzal, M. Maqsood, F. Nazir, U. Khan, F. Aadil, K. M. Awan, I. Mehmood, and O. Y. Song, "A data augmentation-based framework to handle class imbalance problem for Alzheimer's stage detection," *IEEE Access*, vol. 7, pp. 115528–115539, 2019.

[3] J. B. Bae *et al.*, "Identification of Alzheimer's disease using a convolutional neural network model based on T1-weighted magnetic resonance imaging," *Scientific Reports*, vol. 10, no. 1, p. 22252, 2020.

[4] J. Ramya, B. U. Maheswari, M. P. Rajakumar, and R. Sonia, "Alzheimer's disease segmentation and classification on MRI brain images using enhanced expectation maximization adaptive histogram (EEM-AH) and machine learning," *Information Technology and Control*, vol. 51, no. 4, pp. 786–800, 2022.

[5] K. De Silva and H. Kunz, "Prediction of Alzheimer's disease from magnetic resonance imaging using a convolutional neural network," *Intelligence-Based Medicine*, vol. 7, p. 100091, 2023.

[6] C. Feng *et al.*, "Deep learning framework for AD diagnosis via 3D-CNN and FSBi-LSTM," *IEEE Access*, vol. 7, pp. 63605–63618, 2019.

[7] P. Forouzannezhad *et al.*, "A deep neural network approach for early diagnosis of mild cognitive impairment using multiple features," in *Proc. IEEE ICMLA*, 2018, pp. 1341–1346.

[8] S. Ribarič, "Detecting early cognitive decline in Alzheimer's disease with brain synaptic structural and functional evaluation," *Biomedicines*, vol. 11, no. 2, p. 355, 2023.

[9] H. Huang *et al.*, "Voxel-based morphometry and a deep learning model for the diagnosis of early Alzheimer's disease based on cerebral gray matter changes," *Cerebral Cortex*, vol. 33, no. 3, pp. 754–763, 2023.

[10] M. Xu *et al.*, "Preliminary study on early diagnosis of Alzheimer's disease in APP/PS1 transgenic mice using multimodal magnetic resonance imaging," *Frontiers in Aging Neuroscience*, vol. 16, p. 1326394, 2024.

[11] S. Aghajanian *et al.*, "Longitudinal structural MRI-based deep learning and radiomics features for predicting Alzheimer's disease progression," *Alzheimer's Research & Therapy*, vol. 17, no. 1, pp. 1–13, 2025.

[12] D. Mungra *et al.*, "PRATIT: A CNN-based emotion recognition system using histogram equalization and data augmentation," *Multimedia Tools and Applications*, vol. 79, no. 3, pp. 2285–2307, 2020.

[13] B. M. Nguyen *et al.*, "An improved sea lion optimization for workload elasticity prediction with neural networks," *International Journal of Computational Intelligence Systems*, vol. 15, no. 1, p. 90, 2022.

[14] R. Liu *et al.*, "Large margin and local structure preservation sparse representation classifier for Alzheimer's MRI classification," *Frontiers in Aging Neuroscience*, vol. 14, p. 916020, 2022.

[15] V. Adarsh *et al.*, "Multimodal classification of Alzheimer's disease and mild cognitive impairment using custom MKSCDDL kernel over CNN with transparent decision-making," *Scientific Reports*, vol. 14, no. 1, p. 1774, 2024.

[16] F. Segovia *et al.*, "Multivariate analysis of dual-point amyloid PET intended to assist the diagnosis of Alzheimer's disease," *Neurocomputing*, vol. 417, pp. 1–9, 2020.

[17] K. Shankar *et al.*, "Alzheimer detection using Group Grey Wolf Optimization based features with convolutional classifier," *Computers & Electrical Engineering*, vol. 77, pp. 230–243, 2019.

[18] S. Sudha *et al.*, "Segmentation of RoI in medical images using CNN: A comparative study," in *Proc. IEEE TENCON*, 2019, pp. 767–771.

[19] T. S. Sindhu, N. Kumaratharan, and P. Anandan, "Hybrid optimized deep fuzzy clustering-based segmentation and Deep Maxout Network for Alzheimer's disease classification," *Biomedical Signal Processing and Control*, vol. 93, p. 106118, 2024.

[20] K. Tadokoro *et al.*, "Early detection of cognitive decline in mild cognitive impairment and Alzheimer's disease with a novel eye tracking test," *Journal of the Neurological Sciences*, vol. 427, p. 117529, 2021.

[21] T. Zhu, C. Cao, Z. Wang, G. Xu, and J. Qiao, "Anatomical landmarks and DAG network learning for Alzheimer's disease diagnosis," *IEEE Access*, vol. 8, pp. 206063–206073, 2020.

[22] Y. Zhang *et al.*, "Alzheimer's disease multiclass diagnosis via multimodal neuroimaging embedding feature selection and fusion," *Information Fusion*, vol. 66, pp. 170–183, 2021.

[23] T. Zhang *et al.*, "Predicting MCI to AD conversion using integrated sMRI and rs-fMRI: A machine learning and graph theory approach," *Frontiers in Aging Neuroscience*, vol. 13, p. 688926, 2021.

[24] Y. Wang *et al.*, "Transition of mild cognitive impairment to Alzheimer's disease: Medications as modifiable risk factors," *PLOS ONE*, vol. 19, no. 8, p. e0306270, 2024.

[25] J. Zhang *et al.*, "Recent advances in Alzheimer's disease: Mechanisms, clinical trials and new drug development strategies," *Signal Transduction and Targeted Therapy*, vol. 9, no. 1, p. 211, 2024.

[26] M. Sandhya and P. Dhanalakshmi, "Segmentation and classification of Alzheimer's disease using deep fuzzy clustering and deep learning techniques with sea lion optimization algorithm," *Indian Journal of Natural Sciences*, pp. 86187–86195, 2024.